Heliyon 5 (2019) e02396

Contents lists available at ScienceDirect

Heliyon

journal homepage: www.heliyon.com

Predicting the degradation potential of Acid blue 113 by different oxidants using quantum chemical analysis

Anam Asghar [a,*], Mustapha Mohammed Bello [b], Abdul Aziz Abdul Raman [b], Wan Mohd Ashri Wan Daud [b], Anantharaj Ramalingam [3], Sharifuddin Bin Md Zain [d]

[a] Department of Chemical Engineering, University of Engineering & Technology, G.T. Road, Lahore, 54890, Pakistan
[b] Department of Chemical Engineering, Faculty of Engineering, University of Malaya, Kuala Lumpur, 50603, Malaysia
[3] Department of Chemical Engineering, SSN College of Engineering, Chennai, Tamil Nadu, 603110, India
[d] Department of Chemistry, Faculty of Science, University of Malaya, Kuala Lumpur, 50603, Malaysia

ARTICLE INFO

Keywords:
Environmental science
Organic chemistry
Theoretical chemistry
Computational chemistry
Environmental chemistry
Environmental pollution
Acid blue 113 dye
Density functional theory
Hydroxyl radical
Vibrational spectra
Highest occupied molecular orbital
Natural bond orbital

ABSTRACT

In this work, quantum chemical analysis was used to predict the degradation potential of a recalcitrant dye, Acid blue 113, by hydrogen peroxide, ozone, hydroxyl radical and sulfate radical. Geometry optimization and frequency calculations were performed at 'Hartree Fock', 'Becke, 3-parameter, Lee–Yang–Parr' and 'Modified Perdew-Wang exchange combined with PW91 correlation' levels of study using 6-31G* and 6-31G** basis sets. The Fourier Transform-Raman spectra of Acid blue 113 were recorded and a complete analysis on vibrational assignment and fundamental modes of model compound was performed. Natural bond orbital analysis revealed that Acid blue 113 has a highly stable structure due to strong intermolecular and intra-molecular interactions. Mulliken charge distribution and molecular electrostatic potential map of the dye also showed a strong influence of functional groups on the neighboring atoms. Subsequently, the reactivity of the dye towards the oxidants was compared based on the highest occupied molecular orbital (HOMO) and lowest unoccupied molecular orbital (LUMO) energy values. The results showed that Acid blue 113 with a HOMO value -5.227 eV exhibits a nucleophilic characteristic, with a high propensity to be degraded by ozone and hydroxyl radical due to their lower HOMO-LUMO energy gaps of 4.99 and 4.22 eV respectively. On the other hand, sulfate radical and hydrogen peroxide exhibit higher HOMO-LUMO energy gaps of 7.92 eV and 8.10 eV respectively, indicating their lower reactivity towards Acid blue 113. We conclude that oxidation processes based on hydroxyl radical and ozone would offer a more viable option for the degradation of Acid blue 113. This study shows that quantum chemical analysis can assist in selecting appropriate advanced oxidation processes for the treatment of textile effluent.

1. Introduction

Wastewater discharge from food, textile and cosmetic industries contains dyestuffs and other recalcitrant organic contaminants. It is estimated that more than 50,000 tons of different dyes are produced from various industrial processes and approximately 1–10% of them ended up in the wastewater [1]. This results in high levels of chemical oxygen demand (COD) (150–10,000 mg/l), biological oxygen demand (BOD) (100–4000 mg/l), color (50–2500 Pt–Co), suspended solids and toxic organic compounds in textile wastewaters [2, 3, 4].

Commercially available synthetic dyes can be categorized into 20–30 different classes according to their chemical structures [5], out of which 60–70% are classified as azo dyes [6] Among the azo dyes, reactive dyes such as Acid blue 113 (AB113) contribute about 50% to the total market [7] and are extensively used in textile industry due to their high stability [8]. Due to the presence of azo groups (-N=N-), these dyes possess poor biodegradability [9] and exhibit slow degradation [10]. AB113 with two double bonded azo linkage (–N=N–) is kinetically stable. In its structure, each azo group is linked to two carbon atoms, which are part of naphthalene and benzene derivatives. In addition, the aromatic rings in these dyes are toxic and kinetically stable and thus, cause a major problem in wastewater treatment [11]. The International Agency for Research on Cancer (IARC) has classified AB113 as a potential carcinogenic [12].

Conventional methods like adsorption, coagulation, membrane filtration and biological processes have been employed for textile wastewater treatment. These methods are inefficient to degrade

* Corresponding author.
E-mail address: chem.uet@hotmail.com (A. Asghar).

https://doi.org/10.1016/j.heliyon.2019.e02396
Received 31 March 2019; Received in revised form 22 May 2019; Accepted 28 August 2019

recalcitrant organic compounds [13,14]. Alternatively, advanced oxidation processes (AOPs), such as Fenton oxidation [15,16] ozonation [17] and photocatalysis [18] have proven efficient for recalcitrant wastewater treatment. Their effectiveness is due to the production of hydroxyl ($HO^{\bullet}$), ozone (O_3) and sulphate ($SO_4^{\bullet-}$) radicals, which have strong oxidizing abilities [19]. $HO^{\bullet}$, with one electron removed from its configuration, is electronically neutral. However, the unpaired electronic spin configuration makes it unstable and extremely reactive towards oxidative reactions as it tends to capture the missing electron from the interacting molecule [20]. Similarly, $SO_4^{\bullet-}$ with unpaired electron spin configuration is also a strong one-electron oxidant. The O_3 molecule is an unstable triatomic form of oxygen which lacks octet in central oxygen atom. The distribution of electrons along three oxygen atoms is uneven, as central atom must share electrons with either of the attached atoms. The central atom is more deprived of electrons than the outer oxygen atoms. Thus, the central atom has positive charge while either of outer atoms has negative charge, resulting in a dipole force across the entire ozone molecule [21]. Fenton oxidation of AB113 dye has already been performed successfully in our previous works [22,23]. Instances elucidating degradation efficiencies of AB113 dye by processes such as photocatalysis and electrochemical oxidation are also available in the literature [8,24]. These studies have shown that the degree of mineralization depends on the concentration of dye, oxidant and pH of the wastewater. In addition, the chemical reactivity of organic contaminants and oxidants depends on their structural properties, electronic configuration and kinetic stability [25]. In this regard, quantum chemistry could be used to evaluate the reactivity, stability, interaction patterns and structural properties of molecules. Quantum chemical methods usually use the concept of density functional theory (DFT) to predict the chemical behavior and reactivity of chemical species. DFT uses Hohenberg and Kohn theorems to obtain information about energies, structure and properties of chemical species at lower costs compared to the traditional ab-initio wave function techniques [26]. Thus, chemical species can directly be characterized on the basis of their molecular structures [27].

In this work, quantum chemical analysis was performed for AB113 dye in order to predict its degradation potential. Since the choice of computational methods involves a trade-off between accuracy and computational time, three different level of methods and basis sets were compared and analyzed. These include Hartree Fock (HF), Becke-style three-parameter Density Functional Theory with the Lee-Yang-Parr correlation function (B3LYP) and modified Perdew-Wang exchange combined with PW91 correlation (MPW1PW91) methods. The purpose of performing different levels of calculations was to compare and determine the sensitivity of structural and electronic properties of selected molecule to the changes in quantum chemical method. As far as we know, neither quantum chemical calculations nor the vibrational analysis of AB113 dye has been reported. It is pertinent to highlight that few studies have been reported on the use of quantum chemical calculations to investigate quantitative structural activities, reaction kinetics and degradation mechanism of some pollutants. For instance, Liu et al [25] found the relation between the reactivity and structures of six naphthalene sulfonic acid in the Fenton oxidation process. Jia et al [28] developed quantitative structure activity relationship (QSAR) models to study the Fenton oxidation process for 33 different types of pollutants. Guangyou et al [29] studies the degradation mechanism of dimethyldiazene by $HO^{\bullet}$ using DFT/B3LYP/6-31G* level of study. The nature of by-products in the oxidation of organic pollutants is an important consideration since some intermediates may be more toxic than their parent compounds [30]. For AB113, the degradation occurs through the cleavage of the azo double bond (N=N) and the degradation of the aromatic ring [31]. Moura et al [32] identified 1-naphthalenol, 1,6-dimethyl-4-(1-methylethyl)-naphtalene and dibutyl phythalate among the intermediates in the degradation of AB113. Mohammed et al [33] identified 4-diazenyl-1-naphthylamine, 1-naphthyldiazene or 5-diazenyl-1-naphthol as intermediates during the degradation of AB113, which are subsequently mineralized. The intermediate products of the degradation of AB113 are less recalcitrant and are eventually converted to CO_2 and H_2O [34]. Despite these reported studies, the use of quantum chemical calculation to predict the degradation potential of AB113 by different oxidant has not been presented. Although there have been experimental studies on the degradation of AB113 using various AOPs, it is often difficult to make a meaningful comparison due to the varied experimental conditions. Thus, a theoretical approach could provide an alternative to compare the efficacy of different AOPs in degrading AB113. Therefore, the objectives of this study is to investigate: **1)** Geometrical properties of AB113 dye **2)** Structural characterization of AB113 molecule by FTIR and FT-Raman analysis and **3)** Natural bond orbital (NBO) analysis to determine the inter and intra-molecular interactions and 4) Predict the degradation potential of AB113 by different oxidants (H_2O_2, $HO^{\bullet}$, $SO_4^{\bullet-}$ and O_3) through orbital energy analysis. Although AB113 is considered in this work, the approach could be extended to other recalcitrant pollutants.

2. Experimental

AB113 dye was supplied by Sigma-Aldrich (M) Sdn Bhd, Malaysia and was used without further purification. FTIR and FT-Raman spectrum of AB113 was recorded in solid state. The FT-IR spectrum was recorded in the region of 450-4000 cm^{-1} using Perkin Elmer Spectrum 400 FT-IR/FT-FIR (PerkinElmer, UK). The FT-Raman spectrum of AB113 was recorded in the region of 3201-100 cm^{-1} using Renishaw Midel Invia Raman Microscope (Renishaw, UK). The reported spectrums were accurate within ± 1 cm^{-1}.

3. Theory/calculation

3.1. Geometry optimization

The initial geometry of AB113 was generated using **GaussView 05** (Gaussian, Inc., USA) visualization program [35] while quantum chemical calculations were performed using **Gaussian 09W** (Gaussian, Inc., USA) software package [36]. The initial geometry of AB113 was optimized at HF/6-31G* level of study. The geometry obtained at lowest energy minima in the potential energy plot was used for geometry optimization and frequency calculations at higher levels of theory. This study was also planned to perform a comparison among three different levels of theory. For this purpose, HF, B3LYP [37] and MPW1PW91 [38] methods were selected. For further comparison, 6-31G* and 6-31G** were employed as basis sets. Considering the breaking and formation of chemical bonds, un-restricted polarization [39] setting was used for geometry optimization. All calculations were performed using standard gradient techniques and default convergence criteria. The stability of the optimized geometry was confirmed by wavenumber calculations, which gave positive values for all the wavelengths [40].

3.2. Vibrational analysis

In the present study, the vibrational analysis of AB113 was performed in order to assign the experimental vibrational wavenumbers obtained in IR and Raman spectra of AB113. Thus, the Raman intensities for the vibrational frequencies were calculated. Vibrational modes were assigned by means of visual inspection using **GaussView 05 program** [41,42]. The theoretical calculations with unscaled HF and B3LYP force field generally overestimate the frequency of the fundamental modes due to neglect of anharmonicity in real system. These errors can be corrected either by computing anharmonic corrections or by introducing a scaled field or directly scaling the calculated wavenumbers with some scale factor. Thus, the calculated freqeucies are scaled by the scale to the less than 1, to minimize the overall deviation [43,44]. Therefore, the vibrational frequencies obtained at HF method were scaled at 0.9067 and those obtained at DFT method were scaled at 0.958 and 0.983 for the range of wavenumbers above and below 1700 cm^{-1} respectively. After scaling, the deviation from the experimental results should be lesser than

10 cm^{-1} [45].

3.3. Natural bond orbital analysis

The analysis of NBO was conducted with NBO 3.1 program in the **Gaussian 09W** software package. The calculations were conducted to understand the interactions among the filled orbitals and vacant orbitals of subsystems. The interactions between filled and antibonding orbitals represent the deviation from Lewis structure, which can be regarded as a measure of delocalization [46]. These calculations are helpful to analyze the direction of charge transfers and intermolecular bond paths [47]. The stabilization energy ($E^{(2)}$) associated with delocalization is estimated as:

$$E^{(2)} = \Delta E_{ij} = q_i \frac{F(i,j)^2}{\varepsilon_j - \varepsilon_i} \quad (1)$$

Here, i and j are used to represent donor and acceptor. ε_i, and ε_j are the diagonal elements (orbital energies) and F(i, j) is the off-diagonal NBO fock matrix element [46]. With the help of these calculations, it would be possible to predict the charge transfer direction and intermolecular bond paths [47].

3.4. Molecular electrostatic potential (MEP) map

The MEP map, created by nuclei and electrons, are often used to interpret the chemical reactivity of a molecule for electrophilic and nucleophilic attacks. Visualized by GaussView 05 program with different color grading, it is a useful tool to explain the intermolecular interaction between the polar species [48]. Furthermore, it helps to determine the atomic charges within a molecule [49] and define the regions of positive and negative potential through three dimensional map.

3.5. Quantum chemical parameters

The optimized geometries obtained at the selected level of study were used to compute the quantum chemical parameters such as HOMO energy, LUMO energy, HOMO-LUMO energy gap and total electronic energy (E) of the molecules. Based on the frontier molecular orbital (FMO) theory, these energy values are used to predict the chemical reactivity and kinetic stability of a molecule. The HOMO is the orbital that shows the electron donating tendency of a molecule while LUMO being an innermost orbital, exhibits the electron accepting tendency [50].

4. Result and discussions

4.1. Geometry optimization

The geometry optimization of AB113 dye was conducted at ground state using HF/6-31G* level of study. Molecular geometry obtained at energy minima was selected for re-optimization at different levels of study. Consequently, this geometry was optimized using HF, B3LYP and MPW1PW91 methods using 6-31G* and 6-31G** as basis sets. The purpose of using different methods and basis sets was to analyze the sensitivity of calculated optimized geometrical parameters to the changes in the choice of methods and basis sets. The optimized molecular geometry with atom numbering scheme is shown in Fig. 1 while the charges on each atom is provided in supplementary data as Table S1. Comparison of B3LYP and MPW1PW91 methods at 6-31G* and 6-31G** basis sets

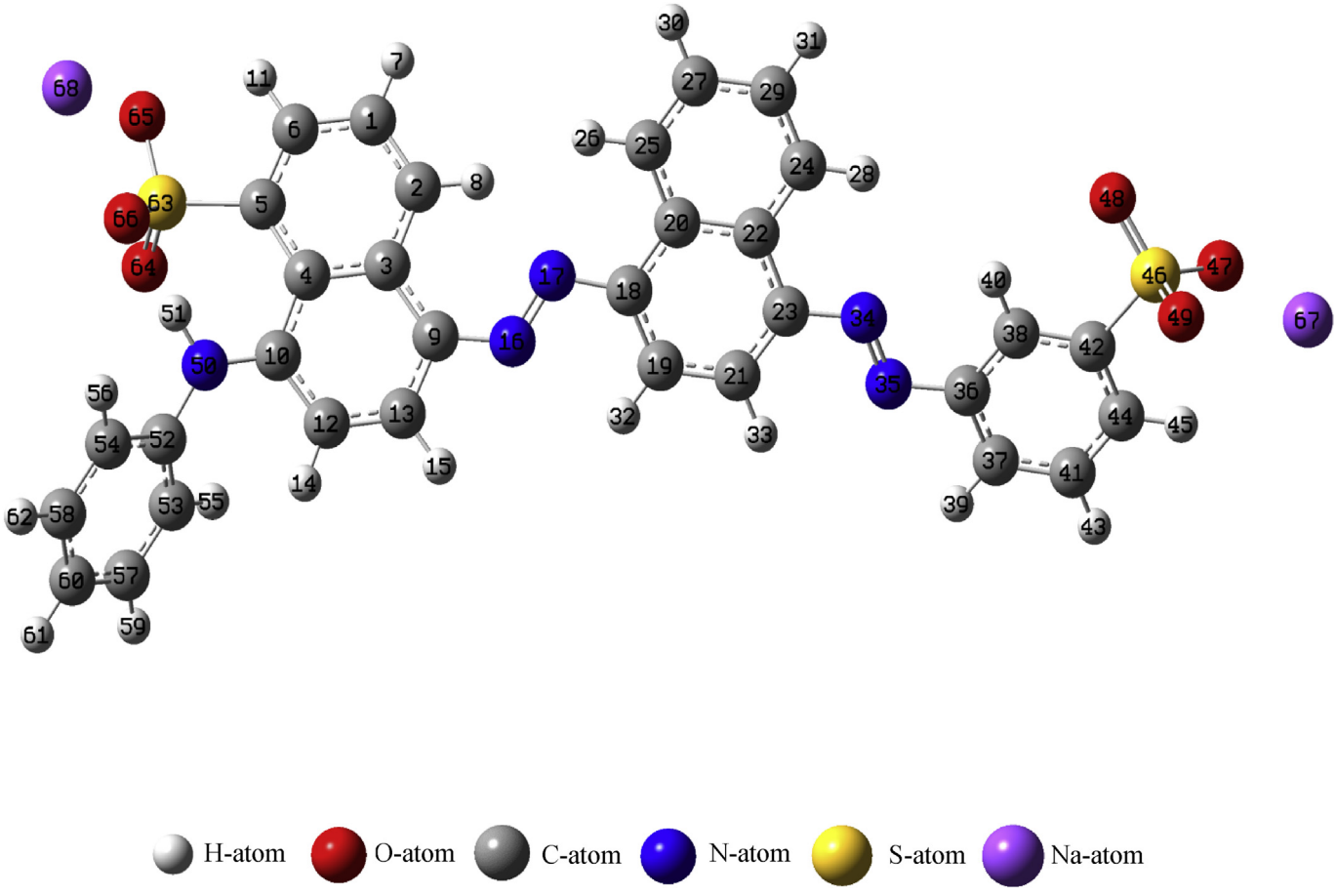

Fig. 1. Optimized geometries of Acid blue 113.

shows a negligible effect on the calculated bond lengths and bond angles. Similarly, the values calculated at HF/6-31G** are similar to those of B3LYP and MPW1PW91 at 6-31G* and 6-31G** basis sets. However, the geometrical parameters calculated at HF/6-31G* level of study showed comparatively shorter bond lengths and angles. This is partly due to the fact that HF does not consider the spin-contamination and therefore, it is not recommended to use for energy calculations [51]. Nevertheless, the geometric parameters obtained at the selected levels of study are in good agreement with each other.

A molecule of AB113 has five C–N, two C–S, six C–O, twenty C–H, thirty-four C–C and one N–H bond lengths. From the theoretical values, it is found that the attachment of N=N and SO_3 groups with benzene rings reduces the electron density within the carbon rings because of the large attraction on valence electron cloud. The benzene ring appears distorted because of the larger bond lengths of C_6–C_5, C_5–C_4, C_4–C_{10}, C_{10}–C_{12}, C_3–C_9, C_{13}–C_9, C_{20}–C_{18}, C_{18}–C_{19}, C_{22}–C_{13}, C_{23}–C_{21}, C_{38}–C_{36}, C_{36}–C_{37}, C_{38}–C_{42} and C_{42}–C_{44}. As a result, the atoms adjacent to these carbon atoms show shorter bond lengths. According to the calculated values, the average C–C and C–H bond lengths are 1.38–1.46 Å and 1.07–1.08 Å respectively. On the other hand, C–N and C–S bond lengths were 1.365–1.414 Å and 1.80–1.83 Å respectively. Furthermore, the bond angles show slight distortions from the hexagonal structure. Based on the optimized geometry, the bond angles within the benzene ring was observed to vary from 119° to over 120°. For instance, angle C_4–C_5–C_6 is calculated at 119°, which is smaller than that obtained for hexagonal structure. These values also indicate that the ring structure is slightly deformed from the hexagonal structure due to the substitution of functional groups for H atom of the benzene rings.

The energy calculations for the optimized structures obtained at selected levels of study show the energy minima values of -1930072.757, -1930097.118, -1938931.976, -1938961.587, -1938636.644, -1938636.644 kcal/mol at HF/6-31G*, HF/6-31G**, B3LYP/6-31G*, B3LYP/6-31G**, MPW1PW91/6-31G* and MPW1PW91/6-31G** respectively. These values indicate that B3LYP method with 6-31G* and 6-31G** basis sets predict the minimum energy configuration for AB113 molecule when compared with other methods and basis sets. Therefore, the B3LYP method was chosen for detailed analysis of the AB113.

4.2. Vibrational analysis

AB113 comprises 58 atoms with 198 normal vibrational modes. Almost all vibrations were observed active in both FTIR and Raman spectra. The values for harmonic wavenumber are always higher than the corresponding experimental quantities due to electron correlation effects and basis set deficiencies. Thus, these values were adjusted after applying some scaling factor as explained earlier. The observed wavenumbers along with IR and Raman intensities and possible assignment with the vibrations of selected molecule are provided in supplementary data as Table S2. Experimentally observed FTIR and Raman spectrum are presented as Fig. 2.

4.2.1. C–C and C=C vibrations

The ring C–C and C=C vibrations are regarded as semicircle vibrations. These vibrations generally appear in the region of 1625-1400 cm^{-1} and 1380-1280 cm^{-1} [52]. In the present investigation, the C–C stretching vibrations are observed in the region of 1598.20-1302.72 cm^{-1} in the FTIR and FT-Raman spectra. However, the calculated frequency values show C–C and C=C stretching vibrations over a wide frequency region of 1670.10-1142.07 cm^{-1}. This slight variation is due to the presence of electronegative atoms such as nitrogen [43,53,54]. Furthermore, the absorption bands arise from out-of-plane bending are occurred in the range of 1059.62–953.20 cm^{-1}, 794.38–396 cm^{-1}. On the other hand, in-plane bendings were observed at 1142.07–1071.21cm^{-1}.

Since AB113 molecule consists of naphthalene rings substituted with

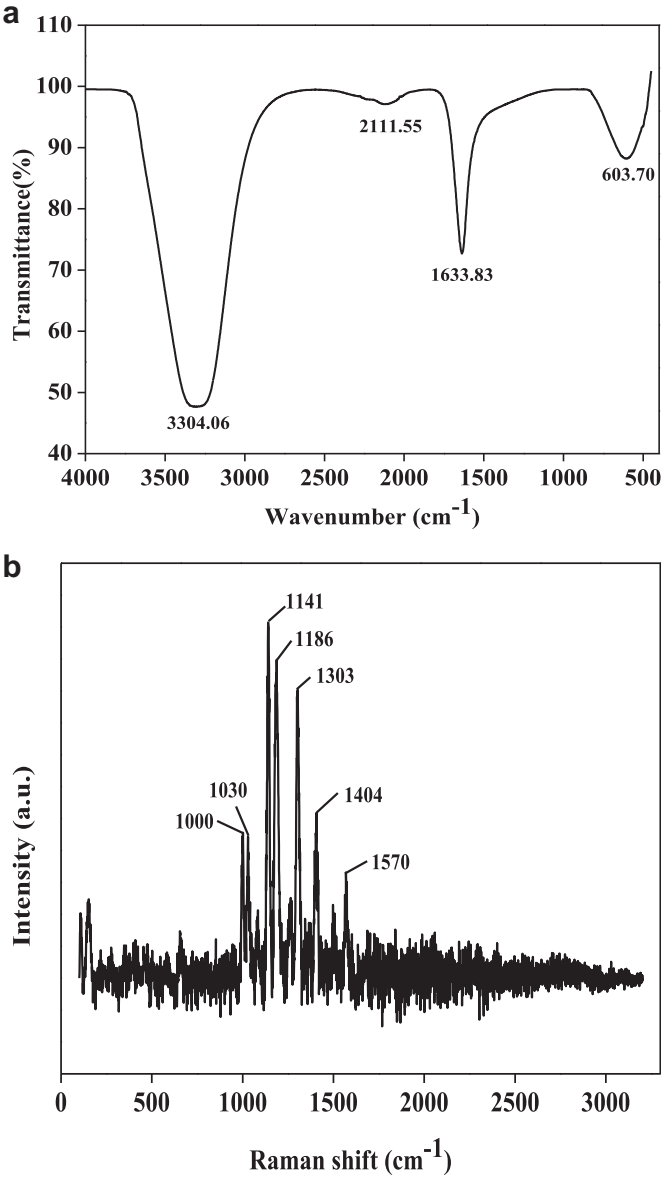

Fig. 2. a) FTIR and **b)** Raman spectra of Acid blue 113.

other naphthalene rings, sulphonic and azo groups, the ring stretching and bending vibrations are observed at very lower frequency values of 333.68, 326.75, 31.61, 304.14-299.65, 41.88–29.46 cm^{-1}. Most of the vibrations were out-of-plane and caused by the substitution of hydrogen atoms by nitrogen, N=N and sulphonic groups. The multiple sharp peaks in FTIR spectrum in the region of 839-490 cm^{-1} represent these vibrations while these absorption bands have less intensity in Raman spectrum. The intensity of these vibrations is represented in the supplementary data as Table S2 and compared in Fig. 2. As observed, these calculated values agree with the experimental, indicating the accuracy of the simulated results.

4.2.2. C–H vibrations

In aromatic compounds, multiple weak bands appear in the region of 3000-3100 cm^{-1} due to the aromatic C–H stretching vibration [55]. It has also been found that benzene-like substituted compounds exhibits C–H stretching, C–H in-plane bending and out-of-plane bending vibrations. In this study, multiple weak bands were observed in the regions of 3200–3000 cm^{-1} and 3000-3100 cm^{-1} in FTIR and FT-Raman spectra

respectively. The C–H asymmetric stretching modes were observed in the range of 3142.5–3156.8, 3170.1–3174.2, 3178.2, 3186.7 and 3198.1 cm^{-1}. On the other hand, C–H symmetric vibrations appear at 3157.7–3166.8, 3178.2, 3186.7, 3190 and 3200.4 cm^{-1}. The calculated values at lower ranges 956.5–943.09, 864.38–843.27 cm^{-1} are due to the out of plane vibrations while 817.37, 803.89 and 966.11 cm^{-1} are assigned for in-plane stretching. The bands obtained at lower values indicate the presence of electron withdrawing groups. The bands appeared with very strong intensity. The in-plane and out of plane bending are also presented in supplementary as Table S2. These observations are in good agreement with the literature and experimentally obtained wavenumber [52,56].

4.2.3. N–H vibrations

In heterocyclic aromatic compounds, N–H vibrations appear in the region of 3000-3500 cm^{-1} [48]. In FTIR spectrum, a medium absorption band observed roughly at 3382.08 cm^{-1} exhibits N–H vibrations. However, the Raman spectrum has no intense peak in the region of 3000 cm^{-1}. Our calculated values showed that presence of N–H molecule in AB113 results in the constant occurrence of absorption bands. This is because N–H has its own frequency and vibrates independently of the other groups in the molecule [48]. A very strong N–H stretching is found at the frequency value of 3299.1 cm^{-1}. The finding of this vibration agrees with the experimental values as observed from Fig. 2 and Table S2 (supplementary data).

4.2.4. C–N and N=N vibrations

The vibrational analysis of AB113 shows that the identification of C–N and N=N stretching is difficult. This is because C–N and N=N vibrations are influenced by the vibrations of other groups attached with them. This results in difficulty in differentiating the wavenumber assigned with C–N and N=N from others. However, data available in literature shows the assignment of C–N vibrations in the region of 2238-1635 cm^{-1} [57,58]. However, for the N=N stretching no such data was found. In IR spectrum of AB113, C–N vibration was observed in the region of 1078-1344 cm^{-1}. However, our calculations show strong N=N vibrations at 1642.05, 1630.08, 1638.36, 1621.54, 1513.73, 1453.97, 1445.79 and 1435.30 cm^{-1}. However, visualization of vibrational modes shows that C–N vibrations were observed in the region of C–C and C=C vibrations.

4.2.5. Sulphonic group vibrations

Generally, the symmetric and asymmetric bands corresponding to sulphonic group appears between 1124-999 cm^{-1} [59]. In IR spectrum, multiple strong bands for S=O are found in the range of 1325–1140 cm^{-1}. However, very weak bands in the region of 512-363 cm^{-1} usually appear corresponding to C–S and S=O vibrations in sulphonate group [60]. In this study, multiple weak absorption bands in the region of 557.14-491.07 cm^{-1} were observed for S=O and C–S functional groups. In Raman, these stretching are missing as no sharp peaks were observed. According to the calculated values, most of the vibrations in sulphonic group appear as a result of carbon rings attached with Sulphur. Thus, very weak and partly strong stretching and vibrations of S=O were found in the regions of 1222.59–1209.77, 1118.08, 1115.65, 989.74, 601.95, 472.59–326.75 cm^{-1}. Out-of-plane bending is assigned at 1097.83 cm^{-1} whereas strong scissoring in-plane bendings were observed at lower values of 568.52–538.21 cm^{-1}. The values obtained at both experimental and theoretical levels agree with each other, indicating the accuracy of our calculations.

4.3. Mulliken charges and natural charge analysis

Mulliken population method is a useful tool for interpreting the reactive behavior of a molecule while performing chemical reaction [61]. Atomic charges calculated by Mulliken population method play a key role in quantum chemical analysis. They are directly related to the vibrational properties of a molecule and are used to describe electronegativity equalization process and charge transfer in chemical reactions [56]. Atomic charges affect the bond lengths, dipole moment, molecular polarizability, electronic structure and are used to define the molecular electrostatic potential surface [62]. The net atomic charge values for AB113 were obtained by the Mulliken charge population analysis, which have been calculated using HF, B3LYP and MPW1PW91 levels of theory with 6–31 G* and 6-31 G** basis sets. The focus here is to compare different methods to characterize the electron distribution in AB113 and sensitivity of calculated charges to the changes in the choice of basis set and the choice of quantum chemical method. The Mulliken charges computed at different methods and basis sets are provided in Table 1. It can be seen that the atomic charges are sensitive to both calculation method and basis set. Thus, considering the calculated atomic charges, the following trend for method basis set was observed:

Quantum chemical method: B3LYP > MPW1PW91 > HF

Basis set: 6-31G** > 6-31 G*

Overall: B3LYP/6-31G** > B3LYP/6-31G* > MP1PW91/6-31G** or MPW1PW91/6-31G* > HF/6-31G** > HF/6-31G*

From Table 1, the most negative atoms were C_1–C_6, C_{12}–C_{13}, N_{16}–N_{17}, C_{19}–C_{22}, C_{24}–C_{25}, C_{27}, C_{29}, N_{34}, N_{35}, C_{37}, C_{38}, C_{41}–C_{42}, C_{44}, O_{47}–O_{49}, N_{50}, C_{53}–C_{54}, C_{57}–C_{58}, C_{60}, and O_{64}–O_{66}. The nitrogen atoms, N_{16}, N_{17}, N_{34}, N_{35} and N_{50} are more negative, which is obvious as these atoms are more electronegative and can easily attract the electrons from the neighbor's atoms. Because of this reason, H_{51} attached to N_{50} possess more positive charge than others because of the more electronegative nature of Nitrogen. Due to the attachment with the more electronegative atom (oxygen), sulphur becomes the most positively charged in sulphonic groups attached to Acid blue 113 molecule. Furthermore, the carbon atoms attached to highly electronegative atoms (nitrogen and sulphur) also show positive charges. This is because the presence of more electronegative atoms abstracts the electrons from their neighbor carbon atoms and make them positive. The result obtained by Mulliken charge analysis are in accordance with the molecular electrostatic potential map and justifies the intermolecular interactions based on the electronegativity of the atoms present in the whole molecular system.

4.4. MEP map

The MEP map explains the charge distribution of the molecule. With these maps it is possible to visualize the charge distributions which can be used to determine how molecules interact with one another. As electrostatic potential map of a molecule is directly linked with the electron density, it provides a better way of predicting the chemical behavior of a molecule. The 3D plot for electrostatic potential map of AB113 is shown in Fig. 3.

In general, different regions on electrostatic potential map are differentiated by different colors i.e. Red, blue, yellow and green. In majority of MEP maps, red color shows maximum negative potential and is a preferred site for electrophilic attacks. The blue color exhibits maximum positive potential and exhibits affinity for nucleophile while green color shows neutral electrostatic region [63]. In this study, MEP map of AB113 obtained at its optimized geometry is almost uniformly green. This suggests that the potential does not change much among benzene rings, azo bonds and sulfonic groups. Molecules with such characteristics neither show affinity for electrophilic attack nor for nucleophilic attack. This is the reason that this molecule is characterized as recalcitrant pollutant whose removal would require the use of highly oxidative and non-selective oxidants.

4.5. NBO analysis

The NBO analysis was conducted to explain inter and intramolecular bonding and interaction among bonds. It is a useful tool for chemical interpretation of hyperconjugative interactions and delocalization of electron density within the molecule [64]. The stabilization of orbital

Table 1
Mulliken charges for Acid blue 113.

Atoms	HF		B3LYP		MP1PW91	
	6-31G*	6-31G**	6-31G*	6-31G**	6-31G*	6-31G**
C_1	-0.217	-0.175	-0.159	-0.109	-0.194	-0.194
C_2	-0.173	-0.095	-0.192	-0.096	-0.211	-0.211
C_3	-0.009	-0.025	0.118	0.103	0.088	0.088
C_4	-0.0321	0.0197	0.099	0.105	0.074	0.074
C_5	-0.335	-0.405	-0238	-0.264	-0.275	-0.275
C_6	-0.210	-0.112	-0.179	-0.115	-0.206	-0.206
H_7	0.238	0.188	0.158	0.113	0.202	0.202
H_8	0.259	0.271	0.259	0.172	0.295	0.295
C_9	0.210	0.172	0.180	0.164	0.173	0.173
C_{10}	0.377	0.244	0.223	0.176	0.229	0.229
H_{11}	0.274	0.214	0.188	0.187	0.228	0.228
C_{12}	-0.262	-0.194	-0.145	-0.087	-0.206	-0.206
C_{13}	-0.193	-0.086	-0.191	-0.106	-0.205	-0.205
H_{14}	0.241	0.179	0.158	0.114	0.211	0.211
H_{15}	0.246	0.1971	0.154	0.109	0.200	0.200
N_{16}	-0.307	-0.304	-0.312	-0.317	-0.309	-0.309
N_{17}	-0.350	-0.452	-0.368	-0.364	-0.391	-0.391
C_{18}	0.262	0.289	0.237	0.219	0.250	0.250
C_{19}	-0.209	-0.151	-0.169	-0.105	-0.202	-0.202
C_{20}	-0.052	-0.038	0.092	0.0819	0.055	0.055
C_{21}	-0.203	-0.129	-0.153	-0.088	-0.183	-0.183
C_{22}	-0.048	-0.0270	0.114	0.098	0.076	0.076
C_{23}	0.263	0.225	0202	0.183	0.204	0.204
C_{24}	-0.199	-0.145	-0.208	-0.141	-0.225	-0.225
C_{25}	-0.197	-0.128	-0.191	-0.116	-0.217	-0.217
H_{26}	0.244	0.176	0.176	0.110	0.222	0.222
C_{27}	-0.219	-0.173	-0.152	-0.108	-0.192	-0.192
H_{28}	0.249	0.202	0.169	0.121	0.212	0.212
C_{29}	-0.219	-0.168	-0.142	-0.099	-0.184	-0.185
H_{30}	0.227	0.180	0.153	0.108	0.197	0.197
H_{31}	0.228	0.179	0.153	0.108	0.197	0.197
H_{32}	0.251	0.201	0.159	0.114	0.205	0.205
H_{33}	0.254	0.202	0.161	0.115	0.206	0.206
N_{34}	-0.340	-0.347	-0.312	-0.312	-0.319	-0.319
N_{35}	-0.310	-0.331	-0.298	-0.296	-0.300	-0.300
C_{36}	0.224	0.189	0.264	0.230	0.242	0.242
C_{37}	-0.191	-0.111	-0.138	-0.078	-0.168	-0.168
C_{38}	-0.176	-0.082	-0.162	-0.0750	-0.179	-0.179
H_{39}	0.247	0.202	0.166	0.121	0.210	0.210
H_{40}	0.278	0.225	0.185	0.135	0.226	0.226
C_{41}	-0.221	-0.172	-0.142	-0.099	-0.184	-0.184
C_{42}	-0.313	-0.345	-0.137	-0.172	-0.193	-0.193
H_{43}	0.241	0.197	0.172	0.127	0.215	0.215
C_{44}	-0.183	-0.108	-0.146	-0.083	-0.173	-0.173
H_{45}	0.257	0.204	0.179	0.132	0.220	0.220
S_{46}	4.682	1.615	1.098	1.100	1.161	1.161
O_{47}	-0.808	-0.865	-0.702	-0.701	-0.722	-0.722
O_{48}	-0.745	-0.867	-0.599	-0.599	-0.613	-0.613
O_{49}	-0.813	-0.773	-0.604	-0.604	-0.617	-0.617
N_{50}	-0.986	-0.818	-0.753	-0.701	-0.780	-0.780
H_{51}	0.465	0.440	0.434	0.378	0.451	0.451
C_{52}	0.365	0.249	0.272	0.227	0.264	0.264
C_{53}	-0.269	-0.194	-0.142	-0.087	-0.203	-0.203
C_{54}	-0.285	-0.201	-0.200	-0.136	-0.235	-0.235
H_{55}	0.225	0.158	0.163	0.111	0.212	0.212
H_{56}	0.221	0.178	0.152	0.105	0.196	0.196
C_{57}	-0.202	-0.144	-0.188	-0.129	-0.218	-0.218
C_{58}	-0.201	-0.156	-0.154	-0.111	-0.195	-0.195
H_{59}	0.218	0.167	0.141	0.096	0.185	0.185
C_{60}	-0.249	-0.193	-0.147	-0.102	-0.192	-0.192
H_{61}	0.213	0.155	0.133	0.087	0.177	0.177
H_{62}	0.219	0.167	0.144	0.099	0.187	0.187
S_{63}	1.729	1.731	1.203	1.231	1.264	1.264
O_{64}	-0.801	-0.742	-0.567	-0.578	-0.576	-0.576
O_{68}	-0.803	-0.822	-0.725	-0.725	-0.755	-0.755
O_{66}	-0.783	-0.772	-0.608	-0.588	-0.621	-0.621
Na_{67}	0.842	0.907	0.855	0.855	0.873	0.873
Na_{68}	0.841	0.863	0.811	0.812	0.837	0.837

interaction is directly proportional to the energy difference between the interacting orbitals [65]. Thus, in order to quantify the molecular interactions, a second order perturbation interaction energy ($E^{(2)}$) was applied as provided by Eq. (1).

Higher values for $E^{(2)}$ indicate intensive interactions between the electron donors and electron acceptors, which will result in greater extent of conjugation. Depending on the types of orbitals, various intra and intermolecular interactions exist within a molecule. For instance, $\pi\rightarrow\pi^*$ interactions result in π conjugation or resonance in benzene ring. On the other hand, primary hyperconjugative interactions occur due to the different types of orbital overlaps such as $\sigma\rightarrow\pi^*$, $\pi\rightarrow\sigma^*$ and secondary hyperconjugative interactions occurs due to $\sigma\rightarrow\sigma^*$ orbital overlaps [66].

The second-order perturbation theory analysis of Fock matrix in the NBO basis of AB113 molecule is presented in supplementary data as Table S3. The natural electronic configuration of atoms obtained as a result of NBO analysis are provided in supplementary data as Table S4a and Table S4b. From the values listed in Table S3, a strong hyperconjugative interactions were observed, which show that the molecule is stable. In AB113, a very strong $\pi^*\rightarrow\pi^*$ interaction was observed between $\pi^*(C_2–C_5)$ and $\pi^*(C_{10}–C_{12})$ with highest $E^{(2)}$ value around 79.53 Kcal/mole. It results in an increase in electron occupancy to 0.19481 and resonance in benzene ring. Similarly, the interactions $\pi(C_1–C_2)\rightarrow\sigma^*$(LP-$C_3$) and σ^*(LP-C_6), $\pi(C_4–C_5)\rightarrow\sigma^*$(LP-$C_3$) and σ^*(LP-C_6), $\pi(C_{10}–C_{12})\rightarrow\sigma^*$(LP-$C_{13}$), $\pi(C_1–C_{23})\rightarrow\sigma^*$(L-$C_{22}$), $\pi(C_{24}–C_{29})\rightarrow\sigma^*$(LP-$C_{22}$), σ^*(LP-C_6)$\rightarrow\pi^*(C_1–C_2)$, σ^*(LP-C_6)$\rightarrow\pi^*(C_4–C_5)$, σ^*(LP-C_{13})$\rightarrow\pi^*(C_{10}–C_{12})$, σ^*(LP-C_{22})$\rightarrow\pi^*(C_{21}–C_{23})$, σ^*(LP-C_{22})$\rightarrow\pi^*(C_{24}–C_{29})$ and interaction initiated by lone pairs (donors) of σ (LP-C_3)$\rightarrow\pi^*(C_1–C_2)$, σ (LP-$C_3$)$\rightarrow\pi^*(C_4–C_5)$, σ (LP-$C_9$)$\rightarrow\pi^*(N_{16}–N_{17})$, σ (LP-$C_{20}$)$\rightarrow\pi^*(C_{18}–C_{19})$, σ (LP-$C_1$)$\rightarrow\pi^*(C_{25}–C_{27})$, n($LP_3O_{48}$)$\rightarrow\sigma^*(S_{46}–O_{49})$, σ(LP-$N_{50}$)$\rightarrow\sigma^*(C_{52}–C_{53})$, π(LP-$O_{64}$)$\rightarrow\sigma^*(S_{63}–O_{66})$, give stabilization to the structure because of their higher $E^{(2)}$ values. However, these intramolecular charge transfer ($n\rightarrow\pi$, $\pi\rightarrow\pi^*$, $\sigma\rightarrow\pi^*$ etc.) may induce non-linearity to the molecule and high intermolecular hyperconjugative interaction around benzene rings and azo groups (N=N) may induce reactivity for oxidants during degradation process [67].

NBO analysis uses natural hybrid orbitals to explain bonding within a molecule. For instance, $\pi^*(N_{34}–N_{35})$ occupies a low energy orbital of 0.7074 a.u. with 99.73% p-character. n_1 (N_{34}) and n_1 (N_{35}) with p-character of 64% and high electron occupancy of 1.97 will donate electrons to $C_{21}–C_{23}$ and $C_{36}–C_{38}$ with low stabilization energy of 3.82 and 4.20 Kcal/mole. On the other hand, n_2 (O_{47}), n_2 (O_{48}), n_2 (O_{49}) occupy low energy orbital with over 99% p –character and high occupation number of ~1.915. On the other hand, π (N_5) with occupies with slightly low electron occupancy of 1.76356 and p character of 83.12%. Thus, a very close to pure p-orbitals will participate for the electron donation to $\sigma^*(S_{46}–O_{48}$, $S_{46}–O_{49})$, $\sigma^*(C_{42}–O_{47}$, $S_{46}–O_{47})$ and $\sigma^*(C_{42}–S_{46}$, $S_{46}–O_{47}$, $S_{46}–O_{48})$ with low stabilization energies of 5.71, 8.61, 6.68, 7.97, 1.18, 9.37 and 3.37 Kcal/mole respectively. The NBO hybrid orbitals with s and p character in % are provided in Table S3.

4.6. Interaction study of Acid blue 113 with different oxidants based on FMO theory

NBO and MEP analyses of AB113 show that the molecule is stable in nature and electrostatically neutral. It means that the charge potential will not change much among benzene rings, azo bonds and sulphonic groups of the AB113. Thus, it will neither show affinity for electrophiles nor for the nucleophiles. Due to such characteristic, AB113 is recalcitrant in nature and therefore, requires highly reactive oxidants for its efficient removal from textile wastewater.

To further confirm the recalcitrant nature of AB113 and its reactivity for the oxidants, quantum chemical parameters such as HOMO energy, LUMO energy and HOMO-LUMO energy gap were considered. Molecules with high HOMO energy favor the reaction with electrophile while those with low LUMO energy show affinity for nucleophiles. The HOMO energy is related to the ionization potential (IP) while LUMO energy is linked with electron affinity (EA). HOMO energy and LUMO energy are used to predict the most reactive position in π-electron systems. The HOMO and LUMO energies for AB113, obtained at the selected level of

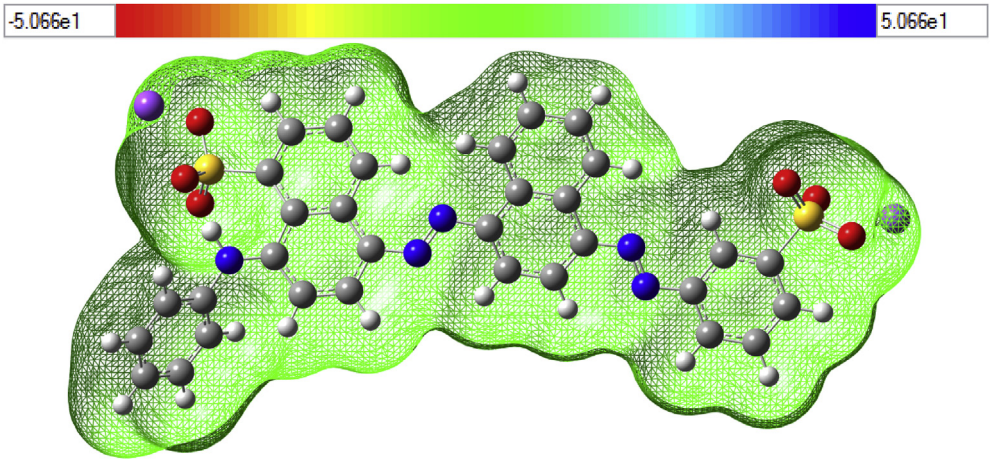

Fig. 3. Molecular electrostatic potential Map of Acid blue 113.

Table 2
HOMO and LUMO energy of Acid blue 113 dye calculated at HF, B3LYP and MPW1PW91 methods.

Methods	HOMO Energy (eV)	LUMO Energy (eV)	HOMO-LUMO Energy gap (eV)
HF/6-31G*	-7.18	0.54	7.71
HF/6-31G**	-7.17	0.54	7.71
B3LYP/6-31G*	-5.23	-2.81	2.42
B3LYP/6-31G**	-5.23	-2.81	2.41
MPW1PW91/6-31G*	-5.54	-2.82	2.72
MPW1PW91/6-31G**	-5.54	-2.82	2.72

studies, are provided in Table 2. Furthermore, the HOMO and LUMO energies along with HOMO-LUMO energy gaps for selected methods are depicted Fig. 4a.

It can be seen, based on the values in Table 2, that AB113 possesses high LUMO energy and low HOMO energy values. A molecule with such properties will be stable in nature as it resists change in its electronic distribution. Furthermore, comparison of methods presented in Fig. 4a shows that B3LYP level with HOMO and LUMO energy values of -5.227 and -2.810/2.814 eV shows the highest results. Also, the results obtained at MPW1PW91 method are also in good agreement with those of B3LYP. Therefore, B3LYP and MPW1PW91 are recommended options for performing quantum chemical calculation of AB113.

Since B3LYP method is suitable for open-shell systems, it was preferred choice to deal with radicals and open-shell system [51]. Thus, H_2O_2, $HO^{\bullet}$, $SO_4^{\bullet-}$ and O_3 were selected as oxidants and computations were performed using B3LYP/6-31G* level of study. The computed quantum chemical parameters obtained are listed in Table 3 and a graphically depicted in Fig. 4b.

Our calculations showed that AB113 with HOMO value of -5.23 eV exhibits nucleophilic character. However, oxidants with comparatively lower HOMO energy were observed to have electrophilic character. This observation was exactly in accordance with Frontier molecular orbital theory, which states that in chemical reaction, HOMO of the reductant acts as an electron donor while LUMO of the oxidant acts as electron acceptor [25]. However, higher values for LUMO energy of the oxidants contradict this statement proposed by FMO.

A molecule with smaller HOMO-LUMO energy gap is more polarizable and reactive in nature. Our calculations showed that hydroxyl radical with lowest energy gap of 4.22 eV is reactive in nature. The results obtained appears to support the electron-donating tendency of AB113 during interaction with the oxidants. Furthermore, sulfate radical with the HOMO-LUMO energy gap of 7.92 eV is the least reactive. On the other hand, O_3 and H_2O_2 show comparative results. This trend is exactly in accordance with that obtained through experimental results observed by several research groups. Thus, based on HOMO-LUMO energy value, the following trend was observed:

HOMO-LUMO energy gap: $HO^{\bullet} > O_3 > SO_4^{\bullet-} > H_2O_2$

It is an established fact that a reaction between two reactants proceeds in a way to produce the most favorable interaction energy. This is controlled by the frontier molecular orbitals of interacting species. Therefore, it is equally important to consider the HOMO-LUMO energy gap of AB113 and the oxidants. The smaller the separation energy value between HOMO of electron donor and LUMO of the acceptor, the stronger will be interaction between interacting orbitals. Due to smaller energy difference of 0.24 eV, the interaction between the HOMO of AB113 and LUMO of the O_3 is the most favorable. On the other hand, the interaction of H_2O_2 with AB113 is least favorable among the selected oxidants because of the large energy difference of 7.32 eV. However, the interaction of $HO^{\bullet}$, which has a low HOMO-LUMO energy value (1.24 eV) and $SO_4^{\bullet-}$, with an intermediate HOMO-LUMO energy value (6.07 eV) indicate their potential to oxidize AB113. The observed higher potential of $HO^{\bullet}$ is in accordance with the values of redox potential of the different oxidants as depicted in Table 4. Many studies have also observed the higher efficacy of $HO^{\bullet}$. For example, Guinea et al [68] reported a higher performance of hydroxyl-mediated oxidation process compared with an ozonation process. Furthermore, Yang et al [69] reported that the higher efficacy of O_3/PMS over PMS or O_3 was due to the production of $HO^{\bullet}$, which confirmed its higher potential over both $SO_4^{\bullet-}$ and O_3. Thus, our theoretical findings are consistent with reported experimental studies. For further clarification, the pictorial description of HOMO-LUMO energy gaps between AB113 and oxidants is presented in Fig. 5.

5. Conclusion

In this study, quantum chemical calculations of AB113 were performed to predict its degradation potential by different oxidants. Geometry optimization and frequency calculations of selected molecules were performed at HF, B3LYP and MPW1PW91 level of study using 6-31G* and 6-31G** basis sets. Comparison of quantum chemical methods showed that B3LYP/6-31G* is the most suitable option for performing quantum chemical calculations. Comparison of observed and theoretically predicted vibrational spectra showed that values obtained

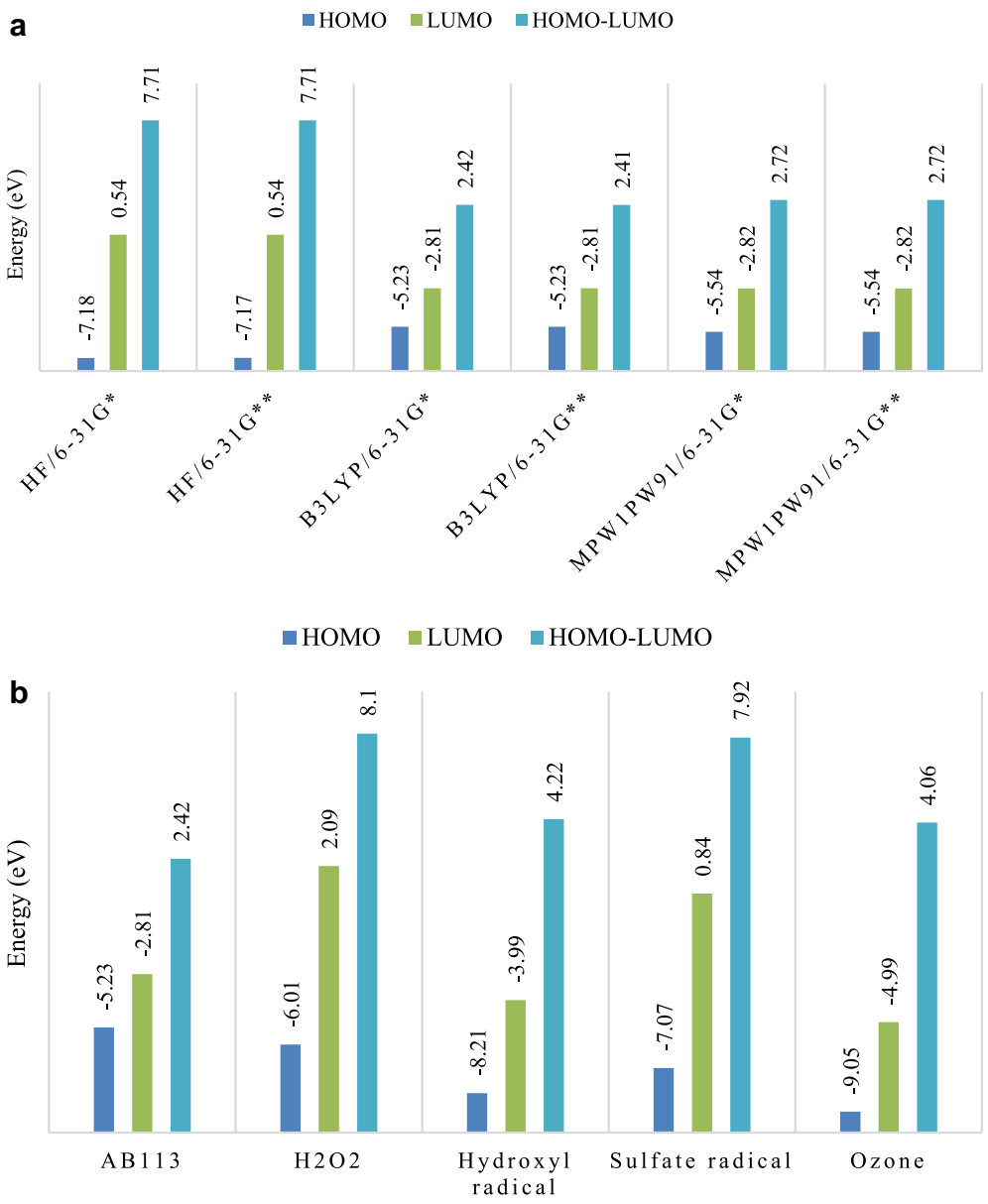

Fig. 4. (a). HOMO energy, LUMO energy and HOMO-LUMO energy gap of Acid blue 113 obtained at different levels of study. **(b)**. HOMO energy, LUMO energy, HOMO-LUMO energy gap of Acid blue 113 and oxidants obtained at B3LYP/6-31G*.

Table 3
Quantum chemical properties of Acid Blue 113 dye and oxidants calculated at B3LYP/6-31G*.

Molecule	Total Energy	HOMO	LUMO	HOMO-LUMO Energy Gap
	(Kcal/mole)	(eV)	(eV)	(eV)
AB113	-1938931.976	-5.23	-2.81	2.42
H_2O_2	95469.363	-6.01	2.09	8.10
Hydroxyl radical	-47708.780	-8.21	-3.99	4.22
Sulfate radical	440427.224	-7.07	0.84	7.92
Ozone	-142000.827	-9.05	-4.99	4.99

at B3LYP/6-31G* are in good agreement with experimentally obtained values. Furthermore, Mulliken charge analysis showed the strong influence of azo bond and sulfonic groups on the neighboring atoms. High stabilization energies obtained through NBO analysis showed that the molecule is stable in nature and delocalization of intra-molecular charge

Table 4
Redox potential of oxidizing agents.

Oxidizing agent	Redox potential (eV)	Reference
$HO^{\bullet}$	2.8	[48]
H_2O_2	1.8	[48,57]
$SO_4^{\bullet -}$	2.5–3.1	[48,58]
O_3	2.1	[48]

transfer is a dominant phenomenon. Moreover, the interaction of AB113 with different oxidants on HOMO-LUMO energy basis showed that AB113 with high HOMO energy value of -5.227 eV exhibits nucleophilic character. The orbital energy analysis of AB113 dye with different oxidants showed that $HO^{\bullet}$ and O_3 have the strongest propensity to oxidize AB113 due to their lower HOMO-LUMO energy gaps of 4.99 and 4.22 eV respectively. Thus, oxidation processes based on $HO^{\bullet}$ and O_3 offer a more viable option for the degradation of AB113. The findings of this study will be useful towards selecting appropriate treatment processes for textile effluents.

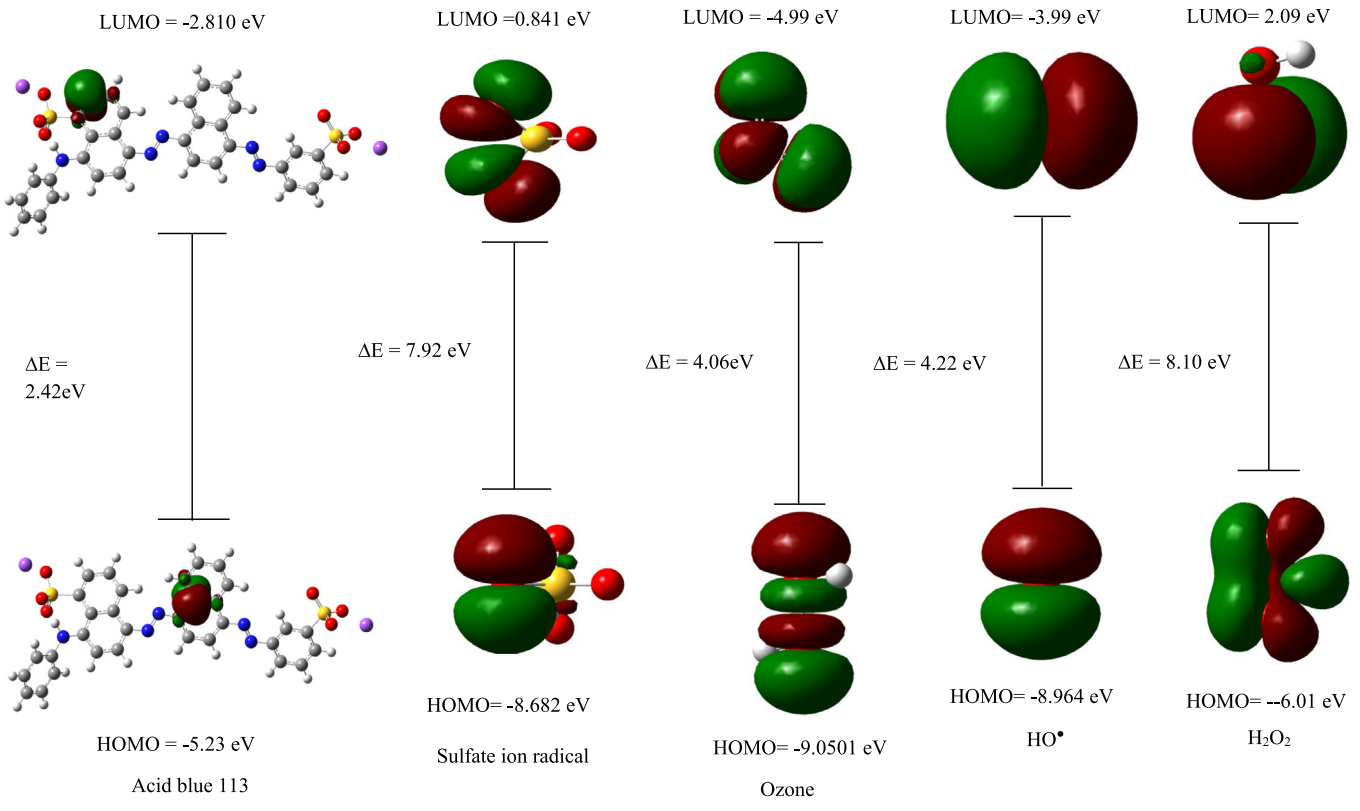

Fig. 5. HOMO energy, LUMO energy, HOMO-LUMO energy gaps of Acid blue 113 and oxidant.

Declarations

Author contribution statement

Anam Asghar: Performed the experiments; Wrote the paper.

Mustapha Mohammed Bello: Analyzed and interpreted the data; Wrote the paper.

Abdul Aziz Abdul Raman: Conceived and designed the experiments.

Wan Mohd Ashri Wan Daud: Contributed reagents, materials, analysis tools or data.

Anantharaj Ramalingam, Sharifuddin Bin Md Zain: Analyzed and interpreted the data.

Funding statement

This work was supported by the RU Geran-Fakulti Program (GPF060A-2018) from University of Malaya and University of Malaya Bright Sparks Unit.

Competing interest statement

The authors declare no conflict of interest.

Additional information

Supplementary content related to this article has been published online at https://doi.org/10.1016/j.heliyon.2019.e02396.

Reference

[1] J. Beltrán-Heredia, J. Sánchez-Martín, M.A. Dávila-Acedo, Optimization of the synthesis of a new coagulant from a tannin extract, J. Hazard. Mater. 186 (2011) 1704–1712.

[2] I. Savin, R. Butnaru, Wastewater Characterization in textile finishing mills, Environ. Eng. Manag. J. 7 (2008) 859–864.

[3] J.C. Akan, F.I. Abdulrahman, J.T. Ayodele, V.O. Ogugbuaja, Impact of tannery and textile effluent on the chemical characteristics of Challawa River, Kano State, Nigeria, Aus. J. Basic Appl. Sci. 8 (2009) 1933–1947.

[4] R. Faryal, A. Hameed, Isolation and characterization of various fungal strains from textile effluent for their use in bioremediation, Pak. J. Bot. 37 (2005) 1003–1008.

[5] M. Lucas, J. Peres, Decolorization of the azo dye Reactive Black 5 by Fenton and photo-Fenton oxidation, Dyes Pigm. 71 (2006) 236–244.

[6] K. Vinodgopal, J. Peller, Hydroxyl radical-mediated advanced oxidation processes for textile dyes: a comparison of the radiolytic and sonolytic degradation of the monoazo dye Acid Orange 7, Res. Chem. Intermed. 29 (2003) 307–316.

[7] D. Rajkumar, J.G. Kim, Oxidation of various reactive dyes with in situ electro-generated active chlorine for textile dyeing industry wastewater treatment, J. Hazard. Mater. 136 (2006) 203–212.

[8] H.S. Lee, P. Parameswaran, A. Kato-Marcus, C.I. Torres, B.E. Rittmann, Evaluation of energy-conversion efficiencies in microbial fuel cells (MFCs) utilizing fermentable and non-fermentable substrates, Water Res. 42 (2008) 1501–1510.

[9] S. Karthikeyan, A. Titus, A. Gnanamani, A.B. Mandal, G. Sekaran, Treatment of textile wastewater by homogeneous and heterogeneous Fenton oxidation processes, Desalination 281 (2011) 438–445.

[10] Mehdi Shirzad-Siboni, K.A.S. Bonilla, A.A.U. de Souza, Removal of COD and color from hydrolyzed textile azo dye by combined ozonation and biological treatment, J. Hazard. Mater. 179 (2010) 35–42.

[11] M. Shirzad-Siboni, S.J. Jafari, O. Giahi, I. Kim, S.-M. Lee, J.-K. Yang, Removal of acid blue 113 and reactive black 5 dye from aqueous solutions by activated red mud, J. Ind. Eng. Chem. 20 (2014) 1432–1437.

[12] World Health Organization International Agency for Research on Cancer, 291ARC: Lyon, France, 1982.

[13] A. Alinsafi, M. Khemis, M.N. Pons, J.P. Leclerc, A. Yaacoubi, A. Benhammou, A. Nejmeddine, Electro-coagulation of reactive textile dyes and textile wastewater, Chem. Eng. Process. 44 (2005) 461–470.

[14] H. Métivier-Pignon, C. Faur-Brasquet, P. Jaouen, P. Le Cloirec, Coupling ultrafiltration with an activated carbon cloth for the treatment of highly coloured wastewaters: A techno-economic study, Environ. Technol. 24 (2003) 735–743.

[15] G.G.P. Anipsitakis, D.D. Dionysiou, Degradation of organic contaminants in water with sulfate radicals generated by the conjunction of peroxymonosulfate with cobalt, Environ. Sci. Technol. 37 (2003) 4790–4797.

[16] K.C. Namkung, A.E. Burgess, D.H. Bremner, H. Staines, Advanced Fenton processing of aqueous phenol solutions: A continuous system study including sonication effects, Ultrason. Sonochem. 15 (2008) 171–176.

[17] J. Nawrocki, B. Kasprzyk-Hordern, The efficiency and mechanisms of catalytic ozonation, Appl. Catal. B. Environ. 99 (2010) 27–42.

[18] Y.-G. Zhang, L.-L. Ma, J.-L. Li, Y. Yu, In situ fenton reagent generated from TiO_2/Cu_2O composite film: a new way to utilize tio_2 under visible light irradiation, Environ. Sci. Technol. 41 (2007) 6264–6269.

[19] A. Asghar, A.A. Abdul Raman, W.M.A. Wan Daud, Advanced oxidation processes for in-situ production of hydrogen peroxide/hydroxyl radical for textile wastewater treatment: a review, J. Clean. Prod. 87 (2015) 826–838.

[20] A. Saed-Mocheshi, H. Pakniyatm H. Pirasteh-Anosheh, M.M. Azooz, Oxidative Damage to Plants, Antioxidant Networks and Signaling, Academic Press, San Diego, 2014, pp. 585–620.

[21] W. Shand, R.A. Spurr, The molecular structure of ozone, J. Amer. Chem. Soc. 65 (1943) 179–181.

[22] A. Asghar, A.A. Abdul Raman, W.M.A. Wan Daud, A comparison of central composite design and taguchi method for optimizing fenton process, Sci. World. J. 2014 (2014) 1–14.

[23] M.M. Bello, A.A. Raman, Performance of fluidized bed fenton process in degrading acid blue 113, IOP Conf. Ser.: Mater. Sci. Eng. 210 (2017) 1–8.

[24] P. Sathishkumar, R.V. Mangalaraja, S. Anandan, M. Ashokkumar, $CoFe_2O_4/TiO_2$ nanocatalysts for the photocatalytic degradation of Reactive Red 120 in aqueous solutions in the presence and absence of electron acceptors, Chem. Eng. J. 220 (2013) 302–310.

[25] H. Liu, Q. Chen, S. Zheng, X. Li, Relationship of mineralization of amino naphthalene sulfonic acids by Fenton oxidation and frontier molecular orbital energies, Chem. Eng. J. 247 (2014) 275–282.

[26] P. Geerlings, F. De Proft, W. Langenaeker, Conceptual density functional theory, Chem. Rev. 103 (2003) 1793–1874.

[27] G. Gece, The use of quantum chemical methods in corrosion inhibitor studies, Corros. Sci. 50 (2008) 2981–2992.

[28] L. Jia, Z. Shen, W. Guo, Y. Zhang, H. Zhu, W. Ji, QSAR models for oxidative degradation of organic pollutants in the Fenton process, J. Taiwan Inst. Chem. Eng. 46 (2015) 140–147.

[29] Z. Guangyou, W. Li, X. Yafei, F. Chunhua, X. Rongshu, The quantum chemical investigation on the important middle product dimethyldiazene in the degredation process of UDMH and •OH, Procedia Environ. Sci. 10 (2011) 703–708.

[30] A. Petrella, G. Mascolo, S. Murgolo, V. Petruzzelli, E. Ranieri, D. Spasiano, D. Petruzzelli, Photocatalytic oxidation of organic micro-pollutants: pilot plant investigation and mechanistic aspects of the degradation reaction, Chem. Eng. Commun. 203 (2016) 1298–1307.

[31] S. Mortazavian, A. Saber, D.E. James, Optimization of photocatalytic degradation of acid blue 113 dye and acid red 88 textile dyes in UV-C/TiO_2 suspension system: Application of response surface methodology (RSM), Catal 9 (2019) 1–19.

[32] D.C.d. Moura, M.A. Quiroz, D.R.d. Silva, R. Salazar, C.A. Martinez-Huitle, Electrochemical degradation of Acid Blue 113 dye using TiO_2-nanotubes decorated with PbO_2 as anode, Environ. Nanotechnol. Monit. Manag. 5 (2016) 13–20.

[33] S. Mohammadzadeh, M.E. Olya, A.M. Arabi, A. Shariati, M.R.K. Nikou, Synthesis, characterization and application of ZnO-Ag as a nanophotocatalyst for organic compounds degradation, mechanism and economic study, J. Environ. Sci. 35 (2015) 194–207.

[34] S. Sekar, S. Mehadevan, B.K. Shanmugam, A.B. Mandal, Bioenergetics and pathway of acid blue 113 degradation by Staphylococcus lentus, Biotechnol. Prog. 28 (2012) 1400–1408.

[35] M.J. Frisch, G.W. Trucks, H.B. Schlegel, G.E. Scuseria, M.A. Robb, J.R. Cheeseman, G. Scalmani, V. Barone, B. Mennucci, G.A. Petersson, H. Nakatsuji, M. Caricato, X. Li, H.P. Hratchian, A.F. Izmaylov, J. Bloino, G. Zheng, J.L. Sonnenberg, M. Hada, M. Ehara, K. Toyota, R. Fukuda, J. Hasegawa, M. Ishida, T. Nakajima, Y. Honda, O. Kitao, H. Nakai, T. Vreven, J.A. Montgomery, J.E. Peralta Jr., F. Ogliaro, M. Bearpark, J.J. Heyd, E. Brothers, K.N. Kudin, V.N. Staroverov, R. Kobayashi, J. Normand, K. Raghavachari, A. Rendell, J.C. Burant, S.S. Iyengar, J. Tomasi, M. Cossi, N. Rega, J.M. Millam, M. Klene, J.E. Knox, J.B. Cross, V. Bakken, C. Adamo, J. Jaramillo, R. Gomperts, R.E. Stratmann, O. Yazyev, A.J. Austin, R. Cammi, C. Pomelli, J.W. Ochterski, R.L. Martin, K. Morokuma, V.G. Zakrzewski, G.A. Voth, P. Salvador, J.J. Dannenberg, S. Dapprich, A.D. Daniels, O. Farkas, J.B. Foresman, J.V. Ortiz, J. Cioslowski, D.J. Fox, Gaussian, Inc., Wallingford CT, 2009.

[36] R. Dennington, T. Keith, J. Millam, Shawnee Mission, KS, Semichem Inc., 2009.

[37] A.D. Becke, Density-functional thermochemistry. III. The role of exact exchange, J. Chem. Phys. 98 (1993) 5648–5652.

[38] J.P. Perdew, Y. Wang, Accurate and simple analytic representation of the electron-gas correlation energy, Phys. Rev. B. 45 (1992) 13244–13249.

[39] M.J. Frisch, J.A. Pople, J.S. Binkley, Self-consistent molecular orbital methods 25. Supplementary functions for Gaussian basis sets, J. Chem. Phys. 80 (1984) 3265–3269.

[40] M. Rocha, A. Di Santo, J.M. Arias, D.M. Gil, A.B. Altabef, Ab-initio and DFT calculations on molecular structure, NBO, HOMO–LUMO study and a new vibrational analysis of 4-(Dimethylamino) Benzaldehyde, Spectrochim. Acta A. Mol. Biomol. Spectrosc. 136 (Part B) (2015) 635–643.

[41] M. Frisch, Gaussview User Manual Gaussian, 2007.

[42] Ö. Mıhçıokur, T. Özpozan, Molecular structure, vibrational spectroscopic analysis (IR & Raman), HOMO-LUMO and NBO analysis of anti-cancer drug sunitinib using DFT method, J. Mol. Struct. 1149 (2017) 27–41.

[43] R. Gayathri, M. Arivazhagan, Vibrational spectroscopy investigation and HOMO, LUMO analysis using DFT (B3LYP) on the structure of 1,3-dichloro 5-nitrobenzene, Spectrochim. Acta A. Mol. Biomol. Spectrosc. 8 (2011) 242–250.

[44] J.S. kumar, S. Jeyavijayan, M. Arivazhagan, Spectroscopic (FT-IR and FT-Raman) investigation, first order hyperpolarizability, NBO, HOMO–LUMO and MEP analysis of 6-nitrochromone by ab initio and density functional theory calculations, Spectrochim. Acta A. Mol. Biomol. Spectrosc. 136 (2015) 771–781.

[45] A. Suvitha, S. Periandy, S. Boomadevi, M. Govindarajan, Vibrational frequency analysis, FT-IR, FT-Raman, ab initio, HF and DFT studies, NBO, HOMO–LUMO and electronic structure calculations on pycolinaldehyde oxime, Spectrochim. Acta A. Mol. Biomol. Spectrosc. 117 (2014) 216–224.

[46] L. Xiao-Hong, T. Zheng-Xin, Z. Xian-Zhou, Natural bond orbital (NBO) population analysis of para-substituted S-Nitroso-thiophenols, J. Mol. Struct. Thermochem. 900 (2008) 50–54.

[47] V.K. Shukla, E.S. Al-Abdullah, A.A. El-Emam, A.K. Sachan, S.K. Pathak, A. Kumar, O. Prasad, A. Bishnoi, L. Sinha, Spectroscopic (FT-IR, FT-Raman, and UV–visible) and quantum chemical studies on molecular geometry, Frontier molecular orbitals, NBO, NLO and thermodynamic properties of 1-acetylindole, Spectrochim. Acta A. Mol. Biomol. Spectrosc. 133 (2014) 626–638.

[48] P. Govindasamy, S. Gunasekaran, Quantum mechanical calculations and spectroscopic (FT-IR, FT-Raman and UV) investigations, molecular orbital, NLO, NBO, NLMO and MESP analysis of 4-[5-(4-methylphenyl)-3-(trifluoromethyl)-1H-pyrazol-1-yl] benzene-1-sulfonamide, J. Mol. Struct. 1081 (2015) 96–109.

[49] S.R. Cox, D.E. Williams, Representation of the molecular electrostatic potential by a net atomic charge model, J. Comput. Chem. 2 (1981) 304–323.

[50] A. Asghar, A.A.A. Raman, W.M.A.W. Daud, A. Ramalingam, Reactivity, stability, and thermodynamic feasibility of H_2O_2/H_2O at graphite cathode: Application of quantum chemical calculations in MFCs, Environ. Prog. Sustain. Energy 37 (4) (2018) 1291–1304.

[51] Q. Xiu-Juan, F. Yong, L. Lei, G. Qing-Xiang, Assessment of Performance of G3B3 and CBS-QB3 Methods in Calculation of Bond Dissociation Energies, Chin. J. Chem. 23 (2005) 194–199.

[52] C. Arunagiri, M. Arivazhagan, M. Subashini, Vibrational spectroscopic (FT-IR and FT-Raman), first-order hyperpolarizablity, HOMO, LUMO, NBO, Mulliken charges and structure determination of 2-bromo-4-chlorotoluene, Spectrochim. Acta A. Mol. Biomol. Spectrosc. 79 (2011) 1747–1756.

[53] V. Udayakumar, S. Peraindy, M. Karabacak, S. Ramalingam, Experimental (FT-IR, FT-Raman) and theoretical (HF and DFT) investigation and HOMO and LUMO analysis on the structure of p-fluoronitrobenzene, Spectrochim. Acta A. Mol. Biomol. Spectrosc. 83 (2011) 575–586.

[54] V. Krishnakumar, R. Ramasamy, Density functional and experimental studies on the FT-IR and FT-Raman spectra and structure of 2,6-diamino purine and 6-methoxy purine, Spectrochim. Acta A. Mol. Biomol. Spectrosc. 69 (2008) 8–17.

[55] G. McMullan, C. Meehan, A. Conneely, N. Kirby, T. Robinson, P. Nigam, I.M. Banat, R. Marchant, W.F. Smyth, Microbial decolourisation and degradation of textile dyes, Appl. Microb. Biotechnol. 56 (2001) 81–87.

[56] M. Arivazhagan, S. Manivel, S. Jeyavijayan, R. Meenakshi, Vibrational spectroscopic (FTIR and FT-Raman), first-order hyperpolarizablity, HOMO, LUMO, NBO, Mulliken charge analyses of 2-ethylimidazole based on Hartree–Fock and DFT calculations, Spectrochim. Acta A. Mol. Biomol. Spectrosc. 134 (2015) 493–501.

[57] M. Arivazhagan, S. Jeyavijayan, J. Geethapriya, Conformational stability, vibrational spectra, molecular structure, NBO and HOMO–LUMO analysis of 5-nitro-2-furaldehyde oxime based on DFT calculations, Spectrochim. Acta A. Mol. Biomol. Spectrosc. 104 (2013) 14–25.

[58] M. Arivazhagan, R. Meenakshi, S. Prabhakaran, Vibrational spectroscopic investigations, first hyperpolarizability, HOMO–LUMO and NMR analyzes of p-fluorobenzonitrile, Spectrochim. Acta. A Mol. Biomol. Spectrosc. 102 (2013) 59–65.

[59] Y. Han, Z. Zheng, C.A. Wang, J. Sun, X. Li, J. Zhang, J. Xiao, G. He, L. Li, A CuII coordination polymer based on incorporated carboxylate and sulfonate groups: Synthesis, crystal structure, and magnetic properties, J. Mol. Struct. 1079 (2015) 163–166.

[60] M.E. Defonsi Lestard, L.A. Ramos, M.E. Tuttolomondo, S.E. Ulic, A. Ben Altabef, Synthesis and vibrational properties of trifluoromethyl trifluoromethanethiosulfonate and comparison with covalent sulfonates, Vib. Spectros. 59 (2012) 40–46.

[61] Z. Demircioğlu, C. Albayrak, O. Büyükgüngör, Theoretical and experimental investigation of (E)-2-([3,4-dimethylphenyl)imino]methyl)-3-methoxyphenol: Enol–keto tautomerism, spectroscopic properties, NLO, NBO and NPA analysis, J. Mol. Struct. 1065-1066 (2014) 210–222.

[62] P. Govindasamy, S. Gunasekaran, S. Srinivasan, Molecular geometry, conformational, vibrational spectroscopic, molecular orbital and Mulliken charge analysis of 2-acetoxybenzoic acid, Spectrochim. Acta. A. Mol. Biomol. Spectrosc. 130 (2014) 329–336.

[63] A. Nataraj, V. Balachandran, T. Karthick, Molecular orbital studies (hardness, chemical potential, electrophilicity, and first electron excitation), vibrational investigation and theoretical NBO analysis of 2-hydroxy-5-bromobenzaldehyde by density functional method, J. Mol. Struct. 1031 (2013) 221–233.

[64] C. Sridevi, G. Velraj, Molecular structure, tautomeric stability, protonation and deprotonation effects, vibrational, NMR and NBO analyses of 2,4-Dioxoimidazolidine-5-acetic acid (DOIAA) by quantum chemical calculations, Spectrochim. Acta A. Mol. Biomol. Spectrosc. 121 (2014) 533–543.

[65] D.M. Gil, M.E. Defonsi Lestard, O. Estévez-Hernández, J. Duque, E. Reguera, Quantum chemical studies on molecular structure, spectroscopic (IR, Raman, UV–Vis), NBO and Homo–Lumo analysis of 1-benzyl-3-(2-furoyl) thiourea, Spectrochim. Acta. A. Mol. Biomol. Spectrosc. 145 (2015) 553–562.

[66] R. Mathammal, N. Sudha, L. Guru Prasad, N. Ganga, V. Krishnakumar, Spectroscopic (FTIR, FT-Raman, UV and NMR) investigation and NLO, HOMO–LUMO, NBO analysis of 2-Benzylpyridine based on quantum chemical calculations, Spectrochim. Acta A. Mol. Biomol. Spectrosc. 137 (2015) 740–748.

[67] L. Sinha, O. Prasad, S. Chand, A.K. Sachan, S.K. Pathak, V.K. Shukla, M. Karabacak, A.M. Asiri, F.T.-I.R. FT-Raman and UV spectroscopic investigation, electronic properties, electric moments, and NBO analysis of anethole using quantum

chemical calculations, Spectrochim. Acta. A. Mol. Biomol. Spectrosc. 133 (2014) 165–177.

[68] E. Guinea, E. Brillas, F. Centellas, P. Canizares, M.A. Rodrigo, C. Saez, Oxidation of enrofloxacin with conductive-diamond electrochemical oxidation, ozonation and Fenton oxidation, A comparison. Water Res. 43 (2009) 2131–2138.

[69] Y. Yang, J. Jiang, X. Lu, J. Ma, Y. Liu, Production of Sulfate Radical and Hydroxyl Radical by Reaction of Ozone with Peroxymonosulfate: A Novel Advanced Oxidation Process, Environ. Sci. Technol. 49 (2015) 7330–7339.